A&A 630, A56 (2019)
https://doi.org/10.1051/0004-6361/201834401

Astronomy & Astrophysics

Is there a non-stationary γ-ray emission zone 42 pc from the 3C 279 core?⋆

V. M. Patiño-Álvarez[1,2], S. A. Dzib[1], A. Lobanov[1,3], and V. Chavushyan[2]

[1] Max-Planck-Institut für Radioastronomie, Auf dem Hügel 69, 53121 Bonn, Germany
e-mail: victorp@inaoep.mx, victorm.patinoa@gmail.com
[2] Instituto Nacional de Astrofísica Óptica y Electrónica (INAOE), Apartado Postal 51 y 216, 72000 Puebla, Mexico
[3] Institut für Experimentalphysik, Universität Hamburg, Luruper Chaussee 149, 22761 Hamburg, Germany

Received 8 October 2018 / Accepted 12 July 2019

ABSTRACT

We investigate the relationship between the variable gamma-ray emission and jet properties in the blazar 3C 279 by combining the *Fermi*-LAT data spanning a period of eight years and concurrent radio measurements made at multiple epochs with VLBA at 15 and 43 GHz within the MOJAVE and VLBA-BU monitoring programmes. The aim of this paper is to compare the flux variability of the different components found in the VLBA observations, to the variability in the gamma-rays. This analysis helps us to investigate whether any of the jet components can be associated with the gamma-ray variability. Through Spearman rank correlation we found that the gamma-ray variability is correlated with a particular region (feature B in the MOJAVE images) downstream from the observed base (core) of the jet. This jet component is therefore a likely location where an important fraction of the variable gamma-ray emission is produced. We also calculated the average proper motion of the component with respect to the VLBA core and found that it moves at an apparent superluminal velocity of $(3.70 \pm 0.35)c$, implying that one of the gamma-ray emission zones is not stationary. This jet component is also found between 6.86 mas and 8.68 mas, which translates to a distance from the radio core of at least 42 pc.

Key words. γ rays: galaxies – radiation mechanisms: non-thermal – quasars: individual: 3C 279 – galaxies: active – techniques: high angular resolution

1. Introduction

Blazars are a class of active galactic nuclei (AGN) whose relativistic jets are pointing very close to the observer's line of sight (Urry & Padovani 1995). At a redshift of 0.5362, 3C 279 is one of the most studied blazars, due to its high brightness, variability, and peculiar optical spectrum (e.g. Torrealba et al. 2012). 3C 279 was also one of the first gamma-ray emitting quasars discovered with the Compton Gamma-Ray Observatory (Hartman et al. 1992). It has been known for decades that this source is highly variable, from radio frequencies (Pauliny-Toth & Kellermann 1966) to gamma-rays (Hartman et al. 1992). For this reason, several intensive multiwavelength campaigns and theoretical studies have led to important revelations about the physical properties of 3C 279 (e.g. Gurwell et al. 2007; Chatterjee et al. 2008; Marscher et al. 2008; Lister et al. 2009, 2013; Smith et al. 2009; Abdo et al. 2010; Richards et al. 2011; Bonning et al. 2012; Nolan et al. 2012; Böttcher et al. 2013; Patiño-Álvarez et al. 2013, 2018; Acero et al. 2015; Jorstad et al. 2017).

3C 279 is a highly variable radio source; however, at radio wavelengths the variability of this source appears to be more moderate than the corresponding variability in the gamma-ray and optical bands during the time period between 2008 and 2010 (Hayashida et al. 2012). The excess variance ($F_{\rm var}$; Vaughan et al. 2003) in the radio regime is quite modest, 0.145 at 37 GHz, 0.165 at 15 GHZ, and 0.104 at 5 GHz, in contrast to the gamma-ray variability of $F_{\rm var} = 0.695$. Hayashida et al. (2015) and Patiño-Álvarez et al. (2018) reported fast gamma-ray variability in 3C 279 during 2013–2014. Several other observational and theoretical studies have been carried out in order to determine both the nature and the stratification of the emission at different bands in 3C 279 (i.e. emission mechanisms and origin of the radiation) (e.g. Lindfors et al. 2006; Larionov et al. 2008; Collmar et al. 2010; Aleksić et al. 2011; Janiak et al. 2012; Hayashida et al. 2012, 2015; Rani et al. 2018). These studies point to the possible presence of multiple emission regions; however, despite these studies, there is still no general consensus about the location of the gamma-ray production zone in 3C 279.

Previous studies have attempted to link the variability in the optical and gamma-ray continuum emission to kinematic changes in Very Long Baseline Interferometry (VLBI) radio images in several individual objects, including 3C 390.3 (Arshakian et al. 2010), 3C 120 (León-Tavares et al. 2010), and 3C 345 (Schinzel et al. 2012). These papers show that the passage of a moving jet component through a stationary shock can trigger flares in emission bands other than the radio.

Thanks to extensive multi-epoch surveys like the 15 GHz Monitoring Of Jets in Active galactic nuclei with VLBA Experiments (MOJAVE[1]; see Lister et al. 2009, 2013) programme and the 43 GHz Boston University VLBA-Blazar monitoring programme (VLBA-BU; see Jorstad et al. 2017), the community has at its disposal a very rich database of VLBA images and reliable measurements of jet proper motions for a number of

⋆ Fluxes of the VLBA components and their simultaneous gamma-ray flux (Tables 2–5) are only available at the CDS via anonymous ftp to cdsarc.u-strasbg.fr (130.79.128.5) or via http://cdsarc.u-strasbg.fr/viz-bin/cat/J/A+A/630/A56

[1] Very Long Baseline Array of the National Radio Astronomy Observatory, Socorro NM, USA.

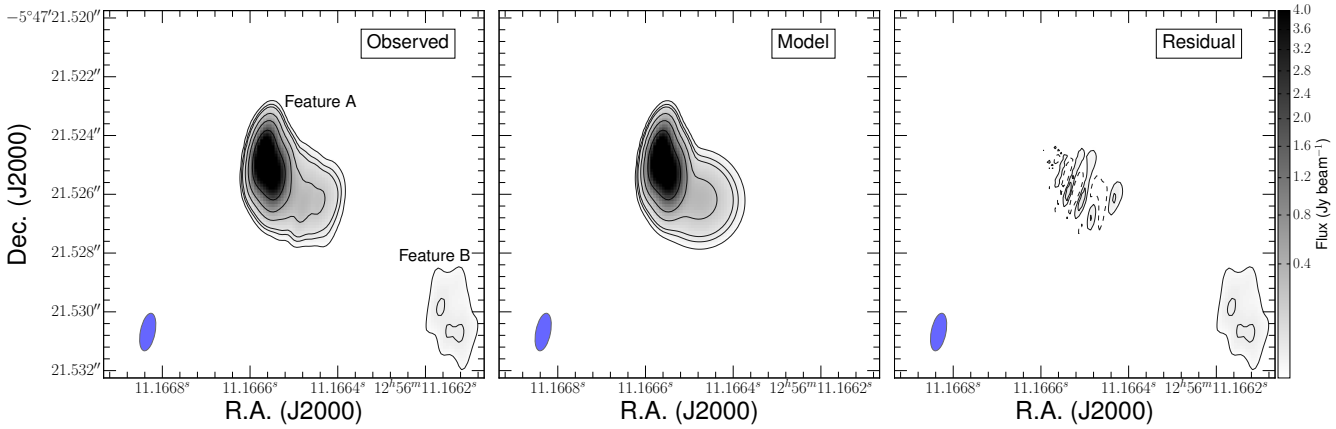

Fig. 1. *Left panel*: 15 GHz VLBA intensity map from the MOJAVE observation of July 16, 2016. *Middle panel*: model of feature A using 2D Gaussian components. *Right panel*: residual image. Feature B is visible in the bottom right corner of the map.

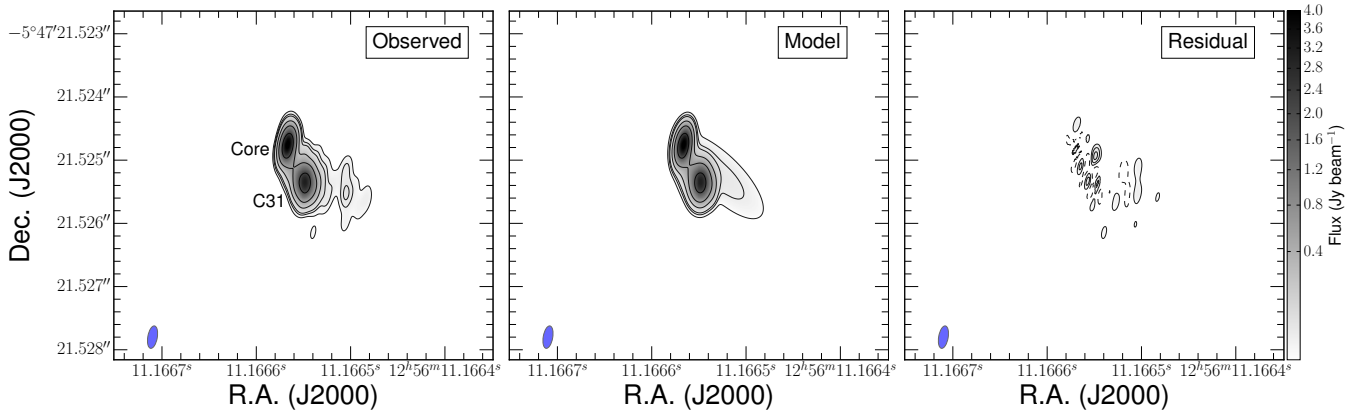

Fig. 2. *Left panel*: 43 GHz VLBA intensity map of 3C 279 from the BU observation of August 26, 2013. *Middle panel*: model of the observed emission using 2D Gaussian components. *Right panel*: residual image.

sources, which allow researching intricate structural changes in parsec-scale jets, e.g. transverse motions, jet acceleration, and other morphological changes.

High angular resolution VLBA observations at 15 and 43 GHz have shown that 3C 279 is a core-dominated blazar, with a complex multicomponent jet structure (see Figs. 1 and 2, and also Lister et al. 2009; Jorstad et al. 2017). In order to investigate whether the distinct emitting regions (jet components) observed in the VLBA maps are related to the gamma-ray emission production, we studied the flux variability of these components and compared it to the variability observed in the gamma-rays.

2. Observations

We used gamma-ray data from the *Fermi* Large Area Telescope (*Fermi*-LAT; Abdo et al. 2009), the VLBA data from the MOJAVE programme (Lister et al. 2009), data from the VLBA-BU programme (Jorstad et al. 2017), and data from the Owens Valley Radio Observatory (OVRO) monitoring programme (Richards et al. 2011). These databases are publicly available. All the dates we present here are in the format $JD_{245} = JD - 2'450'000$.

2.1. Gamma rays

The gamma-ray light curve in the energy range from 0.1 to 300 GeV was built by using data from *Fermi*-LAT. These data were reduced and analysed with the Fermitools version 1.0.2. The region of interest was selected to be 15° radius, centred at the position of 3C 279. The minimization was done through a maximum likelihood algorithm, and the source spectrum was modelled as a log-parabola since it fits the spectrum of 3C 279 better than a power-law model and is also the spectrum type listed in the 4FGL catalogue (Fermi-LAT Collaboration 2019). We included all sources within 15° of 3C 279, extracted from the 4FGL catalogue (Fermi-LAT Collaboration 2019), with their normalization kept free, while sources within 5° had their normalizations and their spectral indices kept free. We applied the currently recommended set of instrument response functions along with the latest diffuse and isotropic background model files. For demonstrations purposes only, the light curve in Fig. 3 was built with a time bin of 7 days in order to increase the S/N, and we kept only the fluxes from time bins with a Test Statistic (TS) > 25 (detection at 5σ or higher). Upper limits were not calculated for the bins with TS < 25 because they are not suitable for correlation analysis. The light curve spans the time range from the launch of *Fermi* in June 2008–February 2017. This light curve is shown in Fig. 3 panel a.

2.2. VLBA 15 GHz observations

The MOJAVE VLBA observations were carried out in 24-h segments at monthly intervals, and in each segment a small subset of the total AGN sample is observed (Lister et al. 2009,

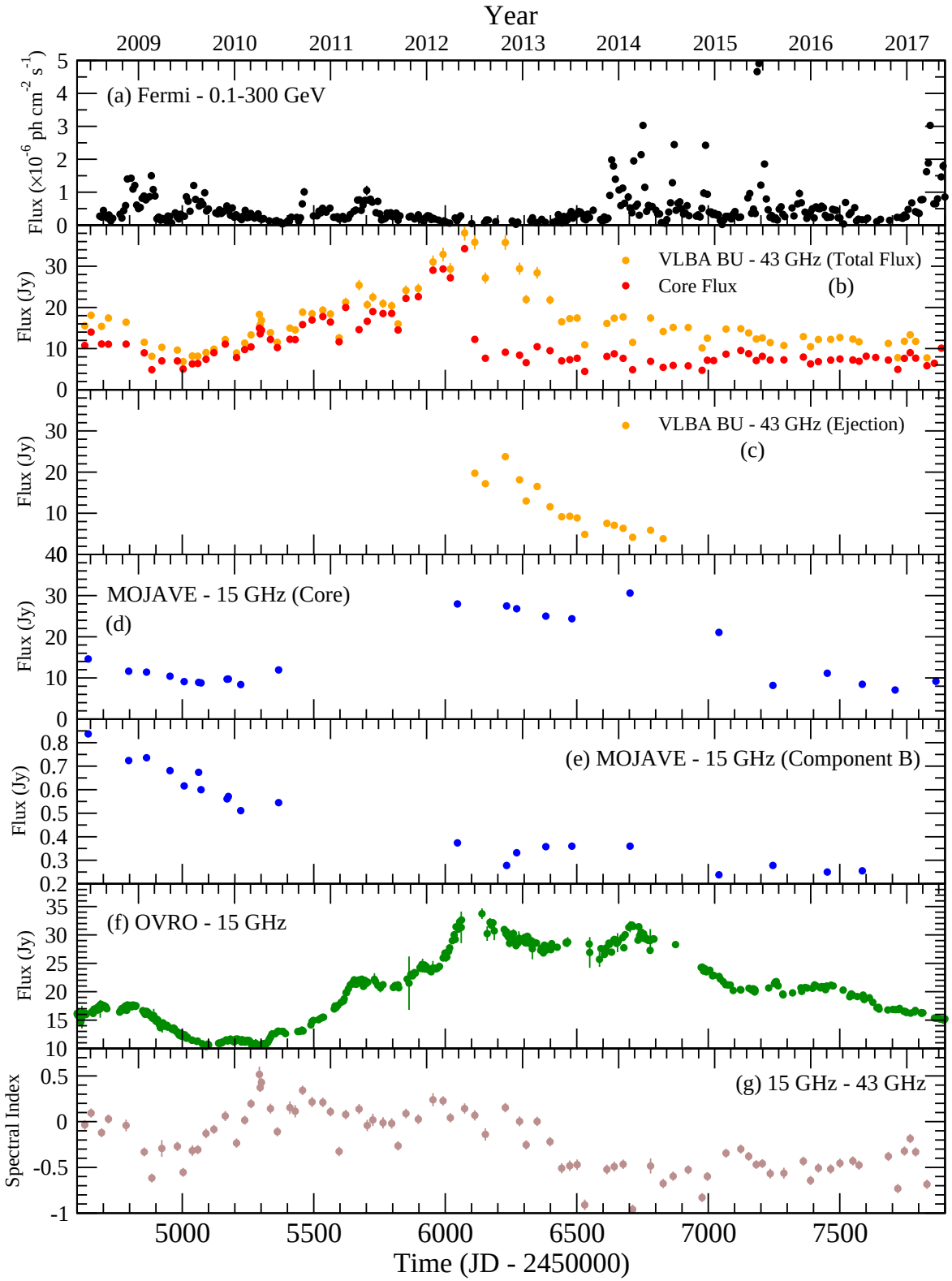

Fig. 3. Multiwavelength light curves of 3C 279. The band of observation and the origin of the data is labelled inside each panel.

2016). The subsets were chosen on the basis of the individual rates of angular jet motion, with several very fast jets (>2 mas yr^{-1}) being observed once per month, while the slowest jets are observed once every few months, as is the case for 3C 279. This resulted in a total of 21 observations of 3C 279 in the time period of the gamma-ray light curve, as described in Sect. 2.1. The natural weighted and non-tapered FITS images were obtained from the MOJAVE website[2].

[2] http://www.physics.purdue.edu/astro/MOJAVE/index.html

The maps used in this work show that there are two main emission features (see Fig. 1); we designate the brightest as feature A and the secondary as feature B. Since feature A is where the radio core is expected to be, we modelled this feature by fitting 2D Gaussian components using the CASA software (McMullin et al. 2007) in order to single out the flux of the radio core at 15 GHz. Modelling feature B was more difficult due to its considerably lower brightness. We were also unable to find consistency in our feature B Gaussian model fits between epochs. Therefore, we carried out our analysis using an integrated value of the flux from feature B. The light curves for the core and the feature B components of the MOJAVE maps are shown in Fig. 3, panels d and e, respectively. For comparison, we also show in Fig. 3, panel f, the light curve of the total flux density at 15 GHz from the OVRO blazar monitoring programme (Richards et al. 2011).

2.3. VLBA 43 GHz observations

The ongoing VLBA-BU programme comprises monthly VLBA observations at 43 GHz. The observations, commenced in June 2007, typically span 24 h during which roughly 33 AGN are observed, with about 45 min spent on each target. There are 84 observations of 3C 279 within the time range of the gamma-ray light curve. The details of this programme, observations, and data reduction are described in Jorstad et al. (2017). The FITS images were obtained from the VLBA-BU programme website[3]. They were also analysed using the CASA software.

As is illustrated in Fig. 2, the total emission in the 43 GHz maps does not come from a single component. In order to characterize the 43 GHz jet structure we used the CASA task IMFIT to model the radio emission using 2D Gaussians. We were able to single out the flux of the core in each map, thus creating a light curve of the core flux, which is shown along with the total flux in Fig. 3 panel b.

Up to the middle of 2012, the flux density of the core clearly dominated the total emission in the 43 GHz maps (see Fig. 3). An ejection of a new jet component is clearly visible in 2013 (see Fig. 2, and Jorstad et al. 2017). During the initial stages this component became brighter than the core, and dominated the total flux density. This component can be tracked over 17 consecutive observations, where it gradually becomes fainter until it is no longer observable. This ejection is labelled C31 in Jorstad et al. (2017), and hereafter we refer to it in this way. The light curve for the flux density of C31 is shown in Fig. 3, panel c. Because of the limited resolution of the 43 GHz VLBA maps (with a beam size of a few parsecs), it is not possible to assess with these observations whether the ejection of C31 actually occurred during mid-2012 or if the core flux measured before was actually a combination of the core and the new jet component.

2.4. OVRO 15 GHz observations

We obtained fully reduced data from the OVRO blazar monitoring programme[4]. Full details of the data reduction and instrument can be found in Richards et al. (2011). The light curve can be seen in panel f of Fig. 3.

[3] https://www.bu.edu/blazars/VLBAproject.html
[4] http://www.astro.caltech.edu/ovroblazars/data/data.php

3. Correlation analysis

In order to understand if any of the features observed in the MOJAVE and BU maps can be directly related to the production of gamma-ray emission, we performed Spearman correlation tests between the simultaneous flux densities of each component with the gamma-ray fluxes. To this end, we calculated gamma-ray fluxes in bins centred at the observation times of the BU and MOJAVE data. We tested incremental bin sizes, starting with the small variability timescales reported in Ackermann et al. (2016) and Pittori et al. (2018), always maintaining the centre as the observation date of the VLBA observations, until the TS for each respective bin was higher than 25.

The relations between the 15 GHz flux densities of the core and feature B of the MOJAVE maps and the calculated simultaneous gamma-ray fluxes (data can be found in Tables 2 and 3, respectively) are shown in the top panels of Fig. 4. The respective relations between the fluxes of the core and the component C31 in the BU maps with the simultaneous gamma-ray fluxes (data can be found in Tables 4 and 5, respectively) are shown in the bottom panels of Fig. 4. The results of the Spearman correlation tests are summarized in Table 1.

We consider a given correlation to be significant if the probability (p-value) of obtaining a specific correlation coefficient by chance is lower than 5% ($p < 0.05$). Under this criterion, only feature B in the MOJAVE maps yields significant correlations (see Table 1). We find a strong and significant correlation between the gamma-ray emission and feature B of the MOJAVE maps, with a correlation coefficient of 0.57. This result can be interpreted as indicating that about 33% of the variability observed in the gamma rays is driven by the variability in the flux density of feature B. In order to discard the possibility that the significant correlations obtained are driven by individual data points we performed a jacknife $n - 1$ analysis (i.e. the correlation is repeated as many times as there are data points available, but discarding a different data point each time). Our results show that, in all cases, the correlation holds significance at a p-value lower than 3%, with correlation coefficients between 0.51 and 0.65, implying strong correlations in all cases. This allows us to confirm that the variability in the gamma rays is related to feature B of the MOJAVE maps. Based on this result, and given that the dominant gamma-ray emission process in this source is found to be inverse Compton scattering (Patiño-Álvarez et al. 2018) we conclude that a gamma-ray emission site is most likely contained within feature B, which is located downstream of the radio core.

4. Spectral index change in the radio emission and the multiwavelength Perspective

The substantial flaring activity observed in 3C 279 during 2012 can be explained by an increase in the Lorentz factor of the jet, which at the same time can cause an increase in the gamma-ray opacity via electron–positron pair production (Patiño-Álvarez et al. 2017, 2018). This matches well with the low emission levels observed in the gamma-ray light curve between 2012 and 2013 (see Fig. 3, panel a).

In order to test whether our hypothesis is true, we combined the total VLBI flux densities at 43 GHz and the 15 GHz OVRO flux densities to estimate the spectral index. Since the 15 GHz light curve is very well sampled, it was interpolated to the epochs of the 43 GHz observations. The resulting 15–43 GHz spectral indices, defined as $S_\nu \propto \nu^\alpha$, are shown in Fig. 3, panel g.

As can be seen in panels b and f of Fig. 3, the variability of the total VLBI flux density at 43 GHz and the 15 GHz emission

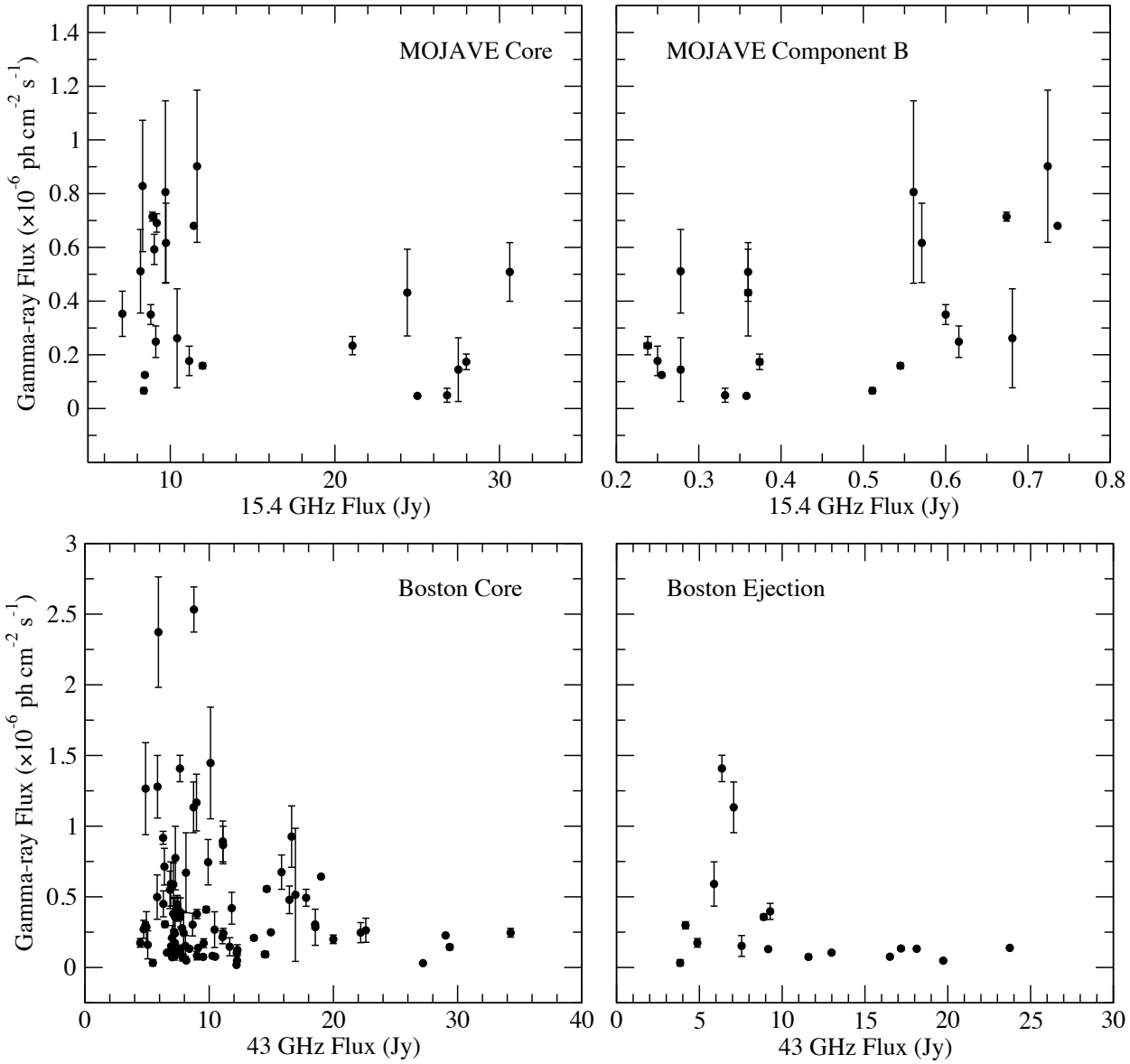

Fig. 4. *Top left panel*: gamma-ray flux vs. radio flux for the core in the MOJAVE maps. *Top right panel*: gamma-ray flux vs. radio flux for component B in the MOJAVE maps. *Bottom left panel*: gamma-ray flux vs. radio flux for the core in the BU-VLBA maps. *Bottom right panel*: gamma-ray flux vs. radio flux for C31 in the BU-VLBA maps.

Table 1. Spearman correlation coefficients obtained between the fluxes of the features in the VLBA maps and the simultaneous gamma-ray fluxes.

VLBA feature	R	R^2	p-value
MOJAVE core	−0.308	0.095	0.143
MOJAVE feature B	0.573	0.328	0.008
BU core	−0.128	0.016	0.231
BU ejection	−0.400	0.160	0.112

(OVRO), match each other very well up to the end of 2012. Afterwards there is a clear decrease in the 43 GHz jet emission (Fig. 3, panel b), while the 15 GHz emission continues to remain active and increases starting around $JD_{245} = 6600$. This causes a decrease in the spectral index around the same epoch.

This change in the spectral index can be a result of a shift in the energy distribution of the electron population to lower energies, which is an expected consequence of the scenario mentioned above. We point out that the spectral index started a decreasing trend approximately at the same time as the onset of decreasing 43 GHz emission ($\sim JD_{245} = 6100-6200$), which supports this scenario.

5. Relative motion between MOJAVE radio components

Since jet feature B is likely to be a gamma-ray emission region, exploring its kinematics can yield further insights into its nature. We were not able to find a prior analysis of its kinematics in the literature. Therefore, we used the VLBA observations from MOJAVE to estimate the proper motion of feature B. It has been demonstrated that this kind of relative positional measurement provides very accurate results (e.g. Rodríguez et al. 2017). To obtain the relative proper motion of feature B, we first determined the position of the brightest spot in feature B using the

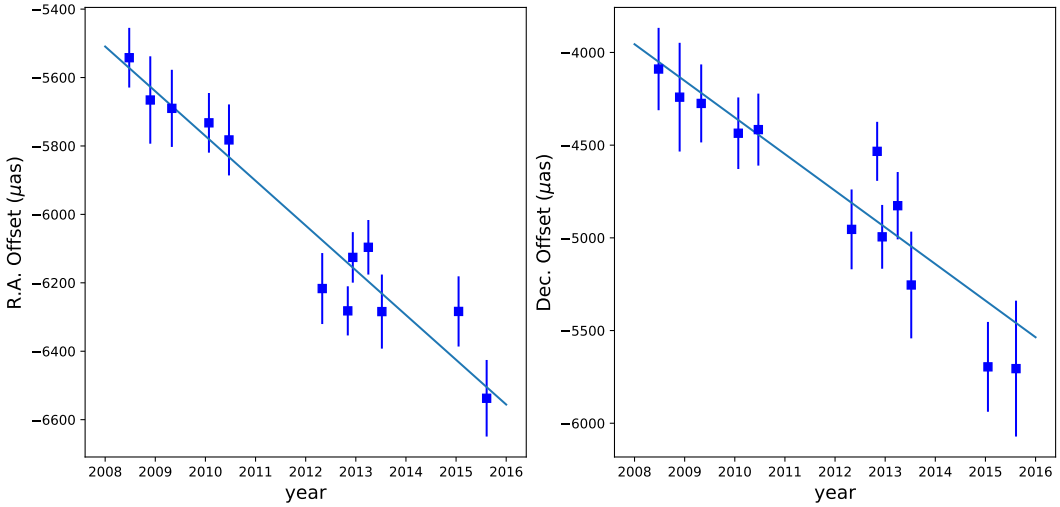

Fig. 5. *Left panel*: separation of feature B from the core, in right ascension, at the different observation epochs. *Right panel*: separation of feature B from the core, in declination, at the different observation epochs. The line represents a chi-square linear fit to the separations, from which we are able to obtain the velocity of feature B.

task IMFIT in CASA. We then subtracted the position of the core from that of feature B at each epoch. Finally, we performed linear fits to the resulting core offset of the feature B in right ascension (RA) and in declination (Dec) in order to estimate the change in position of feature B as a function of time. The measured offsets and the line fits are shown in Fig. 5.

The measured proper motion for feature B in RA is $-130.2 \pm 12.7\,\mu\mathrm{as\,yr^{-1}}$, and in Dec $-130.8 \pm 12.7\,\mu\mathrm{as\,yr^{-1}}$. By applying a cosmology with $H_0 = 73.0\,\mathrm{km\,s^{-1}\,Mpc^{-1}}$, $\Omega_\mathrm{m} = 0.27$, and $\Omega_\Lambda = 0.73$, these proper motions correspond to a total apparent velocity of $(3.70 \pm 0.35)c$. This result implies that the gamma-ray emission site(s) contained within feature B are moving relativistically, which is an important detail when trying to model the gamma-ray emission.

6. Conclusions

We have combined *Fermi*-LAT measurements of the gamma-ray flux in 3C 279 with VLBI images of the parsec-scale structure of the jet and used this combination to identify the likely region responsible for the variable gamma-ray emission in this blazar. We analysed the VLBA data from the MOJAVE survey and the Boston University (BU) monitoring programme. We identified two prominent emission features in the MOJAVE maps. Feature A was modelled and decomposed in order to isolate the core flux. We also modelled the 43 GHz BU maps in order to obtain the core flux, and modelled any distinct emitting regions inside the jet downstream from the core. We identified a component ejected around 2012 (labelled C31 in the analysis of Jorstad et al. 2017) and tracked its evolution over 17 consecutive epochs.

We compared the flux variability of feature B and the core of the MOJAVE maps, as well as the core and component C31 of the BU maps, to that of the gamma-ray emission via a Spearman rank correlation test. Our results imply that feature B is likely related to the variability in the gamma-ray emission. Based on this we suggest that an emission zone responsible for part of the gamma-ray variability is contained within feature B of the MOJAVE maps. This is the first time that a long-lasting gamma-ray emission region has been clearly identified in a parsec-scale map of a blazar.

It is also important to note that the radio component we propose, which may contain a gamma-ray emission zone, is well beyond the central parsec. The measured distances to the MOJAVE feature B go between 6.86 mas and 8.68 mas, which translates roughly to distances between 42 and 54 pc, depending on the cosmology applied.

We find evidence of a change in the spectral index of the radio emission, after a period of low gamma-ray emission. This change of spectral index is expected in the scenario of a shift in the energy distribution of the electron population to lower energies, due to an increase in the cooling via synchrotron emission. This further supports the hypothesis by Patiño-Álvarez et al. (2017, 2018) that an increase in the Lorentz factor of the jet causes an increase in the synchrotron emission, while at the same time increasing the gamma-ray opacity due to electron-positron pair production. This scenario also explains the timing of the spectral index change in the radio emission.

The change in spectral index at radio wavelengths can also be explained by a change in the opacity at radio wavelengths. Since the spectral index moves to negative values after this change, this would mean a decrease in opacity at the lower frequencies; in contrast, an opacity increase would result in a flattening of the spectral index (Kellermann et al. 1988). We also analysed the kinematics of feature B and found that it has a superluminal proper motion of $(3.70 \pm 0.35)c$, which implies that a gamma-ray emission zone within 3C 279 is changing its location with time.

The suggested identification of the gamma-ray emission zone with a region inside the jet in 3C 279 will foster a better understanding of the emission stratification at pc scales. Studies of this kind will also help to improve future modelling attempts for time-resolved spectral energy distribution analysis, since the changes in the model parameters should also be constrained with the information obtained from the broadband light curves and changes observed at parsec-scale.

Acknowledgements. This work was supported by CONACyT research grant 280789 (México). This research has made use of data from the OVRO 40 m monitoring programme (Richards et al. 2011), which is supported in part by NASA grants NNX08AW31G, NNX11A043G, and NNX14AQ89G and NSF grants AST-0808050 and AST-1109911. This research has made use of data from the MOJAVE database, which is maintained by the MOJAVE team (Lister et al.

2009). This study makes use of 43 GHz VLBA data from the VLBA-BU Blazar Monitoring Program (VLBA-BU-BLAZAR; http://www.bu.edu/blazars/VLBAproject.html), funded by NASA through the *Fermi* Guest Investigator Program. The VLBA is an instrument of the Long Baseline Observatory. The Long Baseline Observatory is a facility of the National Science Foundation operated by Associated Universities, Inc.

References

Abdo, A. A., Ackermann, M., Ajello, M., et al. 2009, ApJS, 183, 46
Abdo, A. A., Ackermann, M., Ajello, M., et al. 2010, ApJS, 188, 405
Acero, F., Ackermann, M., Ajello, M., et al. 2015, ApJS, 218, 23
Ackermann, M., Anantua, R., Asano, K., et al. 2016, ApJ, 824, L20
Aleksić, J., Antonelli, L. A., Antoranz, P., et al. 2011, A&A, 530, A4
Arshakian, T. G., León-Tavares, J., Lobanov, A. P., et al. 2010, MNRAS, 401, 1231
Bonning, E., Urry, C. M., Bailyn, C., et al. 2012, ApJ, 756, 13
Böttcher, M., Reimer, A., Sweeney, K., & Prakash, A. 2013, ApJ, 768, 54
Chatterjee, R., Jorstad, S. G., Marscher, A. P., et al. 2008, ApJ, 689, 79
Collmar, W., Böttcher, M., Krichbaum, T. P., et al. 2010, A&A, 522, A66
Fermi-LAT Collaboration 2019, ArXiv e-prints [arXiv:1902.10045]
Gurwell, M. A., Peck, A. B., Hostler, S. R., Darrah, M. R., & Katz, C. A. 2007, in From Z-Machines to ALMA: (Sub)Millimeter Spectroscopy of Galaxies, eds. A. J. Baker, J. Glenn, A. I. Harris, J. G. Mangum, & M. S. Yun, ASP Conf. Ser., 375, 234
Hartman, R. C., Bertsch, D. L., Fichtel, C. E., et al. 1992, ApJ, 385, L1
Hayashida, M., Madejski, G. M., Nalewajko, K., et al. 2012, ApJ, 754, 114
Hayashida, M., Nalewajko, K., Madejski, G. M., et al. 2015, ApJ, 807, 79
Janiak, M., Sikora, M., Nalewajko, K., Moderski, R., & Madejski, G. M. 2012, ApJ, 760, 129
Jorstad, S. G., Marscher, A. P., Morozova, D. A., et al. 2017, ApJ, 846, 98
Kellermann, K. I., & Owen, F. N. 1988, in Radio Galaxies and Quasars, eds. K. I. Kellermann, & G. L. Verschuur, 563
Larionov, V. M., Jorstad, S. G., Marscher, A. P., et al. 2008, A&A, 492, 389
León-Tavares, J., Lobanov, A. P., Chavushyan, V. H., et al. 2010, ApJ, 715, 355
Lindfors, E. J., Türler, M., Valtaoja, E., et al. 2006, A&A, 456, 895
Lister, M. L., Aller, H. D., Aller, M. F., et al. 2009, AJ, 137, 3718
Lister, M. L., Aller, M. F., Aller, H. D., et al. 2013, AJ, 146, 120
Lister, M. L., Aller, M. F., Aller, H. D., et al. 2016, AJ, 152, 12
Marscher, A. P., Jorstad, S. G., D'Arcangelo, F. D., et al. 2008, Nature, 452, 966
McMullin, J. P., Waters, B., Schiebel, D., Young, W., & Golap, K. 2007, in Astronomical Data Analysis Software and Systems XVI, eds. R. A. Shaw, F. Hill, & D. J. Bell, ASP Conf. Ser., 376, 127
Nolan, P. L., Abdo, A. A., Ackermann, M., et al. 2012, ApJS, 199, 31
Patiño-Álvarez, V., Chavushyan, V., León-Tavares, J., et al. 2013, 2012 Fermi Symp. Proc., eConf C121028
Patiño-Álvarez, V. M., Fernandes, S., Chavushyan, V., et al. 2017, FrASS, 4, 47
Patiño-Álvarez, V. M., Fernandes, S., Chavushyan, V., et al. 2018, MNRAS, 479, 2037
Pauliny-Toth, I. I. K., & Kellermann, K. I. 1966, ApJ, 146, 634
Pittori, C., Lucarelli, F., Verrecchia, F., et al. 2018, ApJ, 856, 99
Rani, B., Jorstad, S. G., Marscher, A. P., et al. 2018, ApJ, 858, 80
Richards, J. L., Max-Moerbeck, W., Pavlidou, V., et al. 2011, ApJS, 194, 29
Rodríguez, L. F., Dzib, S. A., Loinard, L., et al. 2017, ApJ, 834, 140
Schinzel, F. K., Lobanov, A. P., Taylor, G. B., et al. 2012, A&A, 537, A70
Smith, P. S., Montiel, E., Rightley, S., et al. 2009, 2009 Fermi Symp. Proc., eConf C091122
Torrealba, J., Chavushyan, V., Cruz-González, I., et al. 2012, Rev. Mex. Astron. Astrofis., 48, 9
Urry, C. M., & Padovani, P. 1995, PASP, 107, 803
Vaughan, S., Edelson, R., Warwick, R. S., & Uttley, P. 2003, MNRAS, 345, 1271